Article

Thermodynamic Assessment of the NaF-KF-UF$_4$ System

Bianca Schacherl [†] **, Rachel Eloirdi, Rudy J. M. Konings** **and Ondrej Beneš** *

Joint Research Centre, European Commission, P.O. Box 2340, 76125 Karlsruhe, Germany;
bianca.schacherl@kit.edu (B.S.); rachel.eloirdi@ec.europa.eu (R.E.); rudy.konings@ec.europa.eu (R.J.M.K.)
* Correspondence: ondrej.benes@ec.europa.eu; Tel.: +49-(0)7247-951-385
† Current address: Karlsruhe Institute of Technology (KIT), Institute for Nuclear Waste Disposal (INE),
P.O. Box 3640, 76021 Karlsruhe, Germany.

Abstract: In the Molten Salt Reactor (MSR) concept, metal fluorides are key components of possible fuel and coolant salts. The fast reactor option opens the possibility for alternatives to the Li based matrix salts, avoiding the costly ^{7}Li enrichment and the tritium production from residual ^{6}Li. Such alternatives can be based on NaF and KF as matrix components. In this study, two pseudo-binary phase diagrams of NaF-UF$_4$ and KF-UF$_4$, and the NaF-KF-UF$_4$ pseudo-ternary system were experimentally investigated using Differential Scanning Calorimetry (DSC). The obtained data were used to perform a full thermodynamic assessment of the NaF-KF-UF$_4$ system. The calculated pseudo-ternary eutectic was found at 807 K and a 68.9-7.6-23.5 mol% NaF-KF-UF$_4$ composition. The comprehensive experimental and modelling data obtained in this work provide further extension of the JRCMSD thermodynamic database describing thermodynamic properties of key fuel and coolant salts for the MSR technology.

Keywords: molten salt reactor fuel; phase diagram; molten fluoride salt; thermodynamics; JRCMSD database

1. Introduction

In the Generation IV initiative, six advanced nuclear reactors were selected as promising candidates for a future nuclear fleet deployment. Among them, the Molten Salt Reactor (MSR) concept was chosen because of its high safety, reliability, and efficiency [1]. These favourable properties are largely due to the use of a homogenous salt mixture that serves as fuel and primary coolant. In the decision process used to select which matrix salt serves the best, important factors including neutronics, melting point, redox potentials, reprocessing scheme, physicochemical properties and economics [2] need to be evaluated carefully.

Many early studies focused on thermal breeder reactors, which included the necessity to use the lithium fluoride based MSR fuel matrix [3]. However, recent developments raised the interest in reactor concepts that enable the use of alternative alkali and earth alkali salts [4]. With those salt mixtures, it is possible to avoid the costly ^{7}Li enrichment and also the in-reactor production of tritium from ^{6}Li residuals (always present in small quantities after enrichment) by neutron capture [5]. The next higher alkali fluorides, NaF and KF, might serve as alternative key matrix components of the MSR fuel to replace LiF. For this reason, the main focus of this study was to extend the existing JRCMSD thermodynamic database [6] by the full assessment of the NaF-KF-UF$_4$ system. With this thermodynamic description, it is possible to predict relevant properties of a multi-component fuel. This includes the melting behaviour, which plays a key role for the safety assessment, but also in economic aspects of MSRs. It is possible to lower the melting temperature of a possible fuel salt mixture, by using a multicomponent fluoride salt [7–10]. These systems are complex and need a well-reviewed comprehensive database to be able to model their physico-chemical behaviour. To obtain the full thermodynamic description of the NaF-KF-UF$_4$ system, thermodynamic optimisations of all related subsystems are necessary.

The NaF-KF pseudo-binary phase diagram was investigated in detail by Kurnakow and Żmcżużnyj [11], Dombrovskaya and Koloskova [12], and Holm [13]. Holm reported an eutectic point of X(KF) = 0.62 mol% [13]. The thermodynamic assessment of the NaF-KF subsystem was presented in our earlier study [14] and the data were further used in this work.

NaF-UF$_4$ phase transitions were first determined from thermal analysis while cooling by Barton et al. [15]. Thoma et al. [16] investigated the phase boundaries in the KF-UF$_4$ system by quenching after equilibration and identification of the phases by powder X-ray diffraction and optical microscopy. Thermal analysis and visual observations were used as supplementary methods.

A first study of the NaF-KF-UF$_4$ system was presented by Thoma et al. [17] based on unpublished thermal analysis data from the period 1950–1958. From their data, the authors derived a preliminary phase diagram but stated that they could not list invariant points because their data did not define the phase relationships [17].

In the current paper, an extensive experimental investigation of the two pseudo-binary phase diagrams for NaF-UF$_4$ and KF-UF$_4$, and a pseudo-ternary investigation of the NaF-KF-UF$_4$ system were performed using Differential Scanning Calorimetry (DSC) and based on the obtained novel phase equilibrium data the full thermodynamic assessment of the NaF-KF-UF$_4$ system was completed. For the NaF-UF$_4$ system, 20 intermediate compositions were synthesised and measured, while for the KF-UF$_4$ system, 21 intermediate compositions were evaluated. Furthermore, 12 different compositions from the pseudo-ternary field were measured for liquidus point determination and used to further optimise the calculated phase diagram.

2. Experimental Section

2.1. Sample Preparation

The commercially obtained compounds used in this study were NaF (99.995 w% metallic purity, source: Alfa Aesar, pr. Nr. 12964) and KF (99.99 w% metallic purity, source: Alfa Aesar, pr. Nr. 10980). Due to the hygroscopic nature of the fluoride compounds, moisture can accumulate during transport. To ensure moisture-free initial end-members, both NaF and KF were heated prior to the mixture synthesis in a Ni crucible under constant argon flow in a tubular furnace at 400 °C for 4 h. The purity was verified by melting point determination using DSC and by XRD powder diffraction phase analysis. As shown in detail in our earlier study [18], both techniques provide complementary purity control of the starting materials. The determined melting points of the end-members agree well with the literature values; for NaF the melting point was determined as 1268 K [19] (ref. value 1269 K) and KF as 1130 K [19] (ref. value 1131 K). The small differences in melting temperatures are within the experimental precision of the applied method. UF$_4$ was synthesised from UO$_2$ by hydro-fluorination with HF using the process described in detail by Souček et al. [18]. First, a U(VI) nitrate solution was electrochemically reduced and precipitated as uranium oxalate. The uranium oxalate was thermally decomposed at 1073 K to UO$_2$ with a large surface area and thus yielding small crystal sizes. This is key to achieve high conversion rates during fluorination. Then, the UO$_2$ was fluorinated at elevated temperatures in a specially designed fluorination apparatus under a constant HF gas flow. The melting point of UF$_4$ was determined to be 1307.7 K, which is in perfect agreement with an earlier determined value from Souček et al. [18]. Furthermore, phase analysis by X-ray diffraction (XRD) showed the presence of UF$_4$. No other phases were detected.

Samples and purified materials were only handled in glove boxes with monitored inert argon atmosphere, with O$_2$ and H$_2$O levels lower than 2 ppm.

2.2. X-ray Diffraction Analyses

A Brucker AXS XRD D8 ADVANCE instrument was used for qualitative powder diffraction analysis to assess the purity of the end-members (as discussed above) and phases in equilibrium of selected pseudo-ternary samples. All XRD measurements were

performed at room temperature. Prior to XRD measurements all samples were embedded in an epoxy glue (Hardmann Double Bubble Red Non Sag 04001 type), which is inert to samples, to protect the sample from O_2 and H_2O absorption from the ambient atmosphere. The absence of interaction of the analyte with the matrix was confirmed using the NaF precursor with three consecutive tests, performed at 10 min, 30 min, and 4 h of total measurement time. No changes in the spectrum with prolonged X-ray irradiation time were visible, which indicates the stability of the prepared sample, as shown in Figure 1. XRD measurements were performed in a glove box under nitrogen atmosphere (<2 ppm O_2 and H_2O).
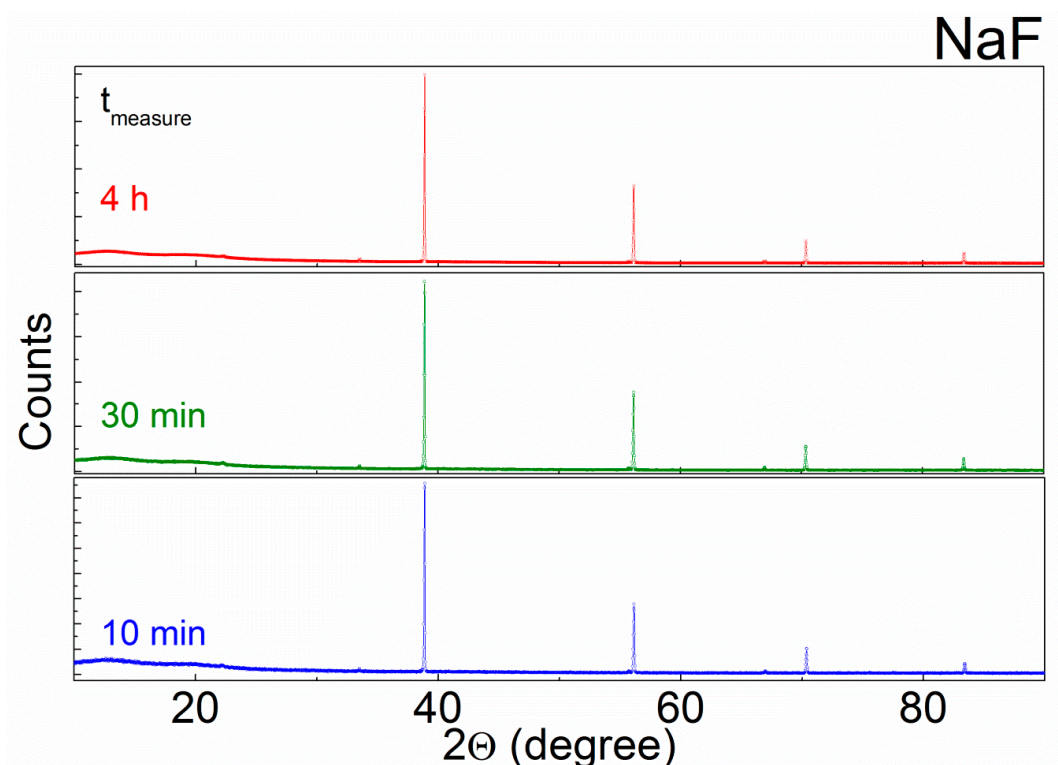

Figure 1. XRD pattern versus time of embedded NaF used in this study for synthesis of fuel mixtures. Plots show stability of the sample prepared under applied conditions at total times of 10 min, 30 min, and 4 h, respectively, as indicated within the figure.

XRD qualitative analyses of the NaF, KF, UF$_4$ end-members, and the pseudo-ternary mixture were performed for a 2Θ range of 20°–120°, with a step size of 0.02° and recording time of 9 s per step. Phases in the sample were identified by comparison to single phase X-ray powder diffraction patterns compiled in the Powder Diffraction File (PDF-2) database [20]. This database is maintained and continually upgraded by the International Centre for Diffraction Data (ICDD). The qualitative analyses was carried out using the ICDD database and Match software, version 1.11f [21].

The calibration of diffraction line positions and shapes determined through powder XRD was performed using the Standard Reference Material (SRM) 660b [22] provided by the National Institute of Standards and Technology (NIST). It consisted of lanthanum hexaboride (LaB$_6$) powder bottled under argon.

2.3. Differential Scanning Caloriemtry for Phase Equilibrium Determination

A pressure resistant stainless steel crucible equipped with a nickel liner and sealed using a procedure described by Beneš et al. [23], ensured precise and reliable measurements of the fluoride mixtures. To realise accurate compositions of the fluoride mixtures, the compounds were mixed in the glove box under argon atmosphere directly in the crucible. The exact weights of each component are given in Tables 1 and 2 in the Appendix A. The

salt specimens were placed in the gas tight crucibles and measured in a Setaram multi-detector high temperature calorimeter (MDHTC 96) with an DSC detector using S-type thermocouples. The DSC detector was calibrated in the range of ca.450 K to ca.1250 K by using pure standard metals (In, Sn, Pb, Al, Ag) for four different heating rates (3 K/min, 5 K/min, 10 K/min, 15 K/min). This calibration curve was applied to the measured phase equilibria of all mixtures. For all measurements, a constant heating rate of 10 K/min was applied with peak temperature of 1525 K, well above the melting point of the highest melting end-member (i.e., UF_4). This heating rate was chosen to ensure consistency in this systematic study. Each measurement consisted of three heating cycles: the first one had a dwell time of 2 h at the maximum temperature to achieve homogeneous mixing of the end-members by melting them together. Therefore, only the second and third heating cycles were used for determination of the phase equilibria. Finally. the obtained equilibrium temperatures of the second and the third cycles were averaged. The variation in the peak shapes can be seen in an exemplary DSC signal in Figure A1 in the Appendix A. The phase transition temperature is derived from tangential analysis of the heat flow signal. The uncertainties differ depending on the shape of the DSC peak as highlighted in our earlier study [24]. Eutectic and peritectic transitions as well as α-β and phase transitions are determined by their onset temperature with an uncertainty of 5 K, while the liquidus transition is determined by the offset temperature, where the uncertainty can be up to 15 K. The phase transition data during cooling is often affected by super cooling effects; therefore, it was only used to verify the number of transitions occurring during crystallisation.

3. Thermodynamic Modelling

The experimental equilibrium data obtained in this work were used as a basis to model the NaF-UF_4 and KF-UF_4 pseudo-binary phase diagrams and the pseudo-ternary phase diagram. The modelling work was carried out according to the Calphad method, which is based on the Gibbs Energy minimisation. All thermodynamic calculations performed in this study were performed using the Factsage v7.1 software [25]. The thermodynamic data for the NaF-KF phase diagram were taken from an optimised phase diagram published in a previous study [14].

3.1. Compounds

The Gibbs energy of the stoichiometric compounds can be described as

$$G(T) = \Delta_f H^0(298) - S^0(298) \cdot T + \int_{298}^T c_p(T) dT - T \cdot \int_{298}^T \frac{c_p(T)}{T} dT, \tag{1}$$

where $\Delta_f H^0(298)$ and $S^0(298)$ are the standard enthalpy of formation and standard absolute entropy both at the reference temperature of 298.15 K and hydrostatic pressure of 1 bar. These thermodynamic parameters were manually optimised in this study for all intermediate compounds for those thermodynamic data that do not exist in the literature. The heat capacity was estimated based on the Neumann-Kopp rule (i.e., the additivity rule for the end-members). Thermodynamic data of all compounds stabilised in the NaF-KF-UF_4 system used in the current assessment are listed in Table 1.

Table 1. Thermodynamic data ($\Delta_f H^{298}$, S^{298}, and $c_P(T)$) of the compounds stabilised in the NaF-UF$_4$, KF-UF$_4$ and NaF-KF-UF$_4$ systems.

Compound	$\Delta_f H^{298}$/kJ mol^{-1}	S^{298}/J K^{-1} mol^{-1}	$c_P(T)$/J K^{-1} mol^{-1}	Reference
NaF (cr.)	−576.65	51.21	$47.63 + 0.01479 \cdot T - 464{,}300 \cdot T^{-2}$	[26]
NaF (liq.)	−557.73	52.76	72.989	[26]
KF (cr.)	−568.61	66.55	$68.757 - 0.05776 \cdot T - 766718 \cdot T^{-2} + 7.5405 \cdot 10^{-5} \cdot T^2 - 2.3886 \cdot 10^{-8} \cdot T^3$	[18]
KF (liq.)	−554.37	67.77	71.965	[18]
UF$_4$ (cr.)	−1914.20	151.70	$114.519 + 0.02055 \cdot T - 413{,}159 \cdot T^{-2}$	[27]
UF$_4$ (liq.)	−1914.66	115.40	174.74	[27]
Na$_2$[UF$_6$] (cr.)	−3095.98	265.30	$209.779 + 0.05013 \cdot T - 1{,}341{,}759 \cdot T^{-2}$	This study
Na$_3$[UF$_7$] (α−cr.)	−3649.90	347.30	$257.409 + 0.06492 \cdot T - 1{,}806{,}059 \cdot T^{-2}$	This study
Na$_3$[UF$_7$] (β−cr.)	−3649.40	347.91	$257.409 + 0.06492 \cdot T - 1{,}806{,}059 \cdot T^{-2}$	This study
Na[U$_2$F$_9$] (cr.)	−4434.45	350.90	$276.669 + 0.055900 \cdot T - 1{,}290{,}618 \cdot T^{-2}$	This study
Na$_5$[U$_3$F$_{17}$] (cr.)	−8690.25	757.40	$581.708 + 0.135615 \cdot T - 3{,}560{,}977 \cdot T^{-2}$	This study
Na$_7$[U$_6$F$_{31}$] (cr.)	−15,715.139	1255.984	$1020.526 + 0.22686 \cdot T - 5{,}729{,}054 \cdot T^{-2}$	This study
K$_2$[UF$_6$] (α−cr.)	−3092.856	318.97	$252.034 - 0.094959 \cdot T - 1{,}946{,}596 \cdot T^{-2} + 1.5081 \cdot 10^{-4} \cdot T^2 - 4.77713 \cdot 10^{-8} \cdot T^3$	This study
K$_2$[UF$_6$] (β−cr.)	−3092.36	319.56	$252.034 - 0.094959 \cdot T - 1{,}946{,}596 \cdot T^{-2} + 1.5081 \cdot 10^{-4} \cdot T^2 - 4.77713 \cdot 10^{-8} \cdot T^3$	This study
K$_3$[UF$_6$] (cr.)	−3668.41	404.34	$320.791 - 0.15272 \cdot T - 2{,}713{,}314 \cdot T^{-2} + 2.2621 \cdot 10^{-4} \cdot T^2 - 7.16569 \cdot 10^{-8} \cdot T^3$	This study
K[U$_2$F$_9$] (cr.)	−4434.01	382.95	$297.796 - 0.016647 \cdot T - 1{,}593{,}036 \cdot T^{-2} + 7.54049 \cdot 10^{-5} \cdot T^2 - 2.38856 \cdot 10^{-8} \cdot T^3$	This study
K$_7$[U$_6$F$_{31}$] (cr.)	−15,680.03	1486.03	$1168.418 - 0.28097 \cdot T - 7{,}845{,}982 \cdot T^{-2} + 5.27834 \cdot 10^{-4} \cdot T^2 - 1.67199 \cdot 10^{-7} \cdot T^3$	This study
NaKUF$_6$ (cr.)	−3,114,000	269.46	$230.907 - 0.022412 \cdot T - 1{,}644{,}177 \cdot T^{-2} + 7.540486 \cdot 10^{-5} \cdot T^2 - 2.38856 \cdot 10^{-8} \cdot T^3$	This study
Na$_2$KUF$_7$ (cr.)	−3,700,000	320.67	$278.537 - 0.007622 \cdot T - 2{,}108{,}477 \cdot T^{-2} + 7.540486 \cdot 10^{-5} \cdot T^2 - 2.38856 \cdot 10^{-8} \cdot T^3$	This study

3.2. Solutions

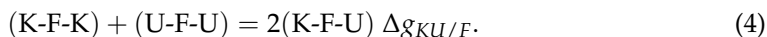The Gibbs energy of a binary solution can be described as

$$G(T) = G^0(T) + \Delta G^{id} + \Delta G^{xs}, \tag{2}$$

where $G^0(T)$ is the standard Gibbs free energy of the mixing end-members, ΔG^{id} is the ideal mixing term, and ΔG^{xs} is the excess Gibbs energy function.

The solid solutions in the NaF-KF system have been assessed earlier [14], and neither the NaF-UF$_4$ nor the KF-UF$_4$ system contain solid solutions. Thus, the only solution, which was subjected to thermodynamic assessment in this study, was the liquid solution. We note here that it is also likely that partial or full solubility in the solid state might occur between Na$_6$U$_7$F$_{31}$ and K$_6$U$_7$F$_{31}$, and between NaU$_2$F$_9$ and KU$_2$F$_9$; however, since we could not experimentally address the presence of such solution(s), we did not include them in the assessment of the NaF-KF-UF$_4$ pseudo-ternary system. This area may require further attention in future studies.

The excess Gibbs energy parameters of the liquid solution were described by the modified quasi-chemical model with a quadruplet approximation [28,29]. This is on the one hand claimed a suitable model for describing ionic liquids, and on the other

hand, it allowed us to maintain compatibility with the extensive JRCMSD thermodynamic database [6] describing fluoride and chloride salt systems. The basis of this quadruplet is a polynomial formalism using the excess Gibbs energy parameters for the second nearest neighbour pair-exchange reaction:

$$(Na\text{-}F\text{-}Na) + (U\text{-}F\text{-}U) = 2(Na\text{-}F\text{-}U) \; \Delta g_{NaU/F}, \tag{3}$$

$$(K\text{-}F\text{-}K) + (U\text{-}F\text{-}U) = 2(K\text{-}F\text{-}U) \; \Delta g_{KU/F}. \tag{4}$$

As an example, for the NaF-UF$_4$, system the $\Delta g_{NaU/F}$ parameter can be expanded as a polynomial:

$$\Delta g_{\frac{NaU}{F}} = \Delta g^0_{\frac{NaU}{F}} \sum_{(i+j) \geq q^1} g^{ij}_{\frac{NaU}{F}} \chi^i_{\frac{NaU}{F}} \chi^j_{\frac{UNa}{F}}. \tag{5}$$

Furthermore, the model requires definition of a composition of the strongest short range ordering. This is achieved by defining cation-cation coordination numbers $Z^{i,j}_{ij}$, in which *i* and *j* are the mixing cations. At this composition, the excess Gibbs energy of the liquid solution tends to have its minimum and thus is generally related to the eutectic point, i.e., to the lowest melting region. The coordination numbers are composition and temperature independent, and they are defined during the phase diagram optimisation. The selected coordination numbers used in this study are listed in the Table 2 below:

Table 2. Cation-cation coordination numbers $Z^{i,j}_{ij}$, for the mixing cations *i* and *j* used for the thermodynamic modelling.

i	j	$Z^{i,j}_{ij}$	$Z^{i,j}_{ij}$
Na	U	3	6
K	U	3	6

To maintain electro neutrality in the system, once the cation-cation coordination numbers are selected the anion coordination numbers are calculated according to the following equation:

$$\frac{q_i}{Z^i_{ij/FF}} + \frac{q_j}{Z^j_{ij/FF}} = \frac{2q_F}{Z^F_{ij/FF}}.$$

The excess Gibbs energy parameters $\Delta g^0_{NaU/F}$ and $g^{ij}_{NaU/F}$ were obtained by optimisation of the experimental data of the (Na,U)F$_x$ and (K,U)F$_x$ liquid solutions and the obtained values are given below (in J·mol^{-1}):

$$g^{00}_{NaU} = -25104 + 4.184 \cdot T, \tag{6}$$

$$g^{10}_{NaU} = -26961 + 18.184 \cdot T, \tag{7}$$

$$g^{01}_{NaU} = -40200 + 32.276 \cdot T, \tag{8}$$

$$g^{00}_{KU} = -30304, \tag{9}$$

$$g^{10}_{KU} = -15101 + 4.866 \cdot T, \tag{10}$$

$$g^{01}_{KU} = -5417 - 5.276 \cdot T. \tag{11}$$

The $\chi_{NaU/F}$ term from Equation (5) was determined by the composition of the solution; here, X_{NaNa}, X_{NaU}, and X_{UU} represent the cation-cation pair mole fractions, given by

$$\chi_{NaU/F} = \frac{X_{NaNa}}{X_{NaNa} + X_{NaU} + X_{UU}}. \tag{12}$$

All optimisations of the excess Gibbs parameters of the liquid solution and the thermodynamic data of the intermediate phases (as discussed above) were carried out using

the so-called trial-error method until good agreement between the experimental data and the calculation was achieved.

For the pseudo-ternary system calculation, the mixing cations were subdivided into two groups: (i) first containing the highly ionic Na and K constituents and (ii) the second one containing U constituents with a more molecular-type behaviour. Taking this into account, the asymmetric Kohler-Toop formalism was used to extrapolate the excess Gibbs parameters of the pseudo-ternary solutions of the NaF-KF-UF$_4$ phase diagram from its pseudo-binary sub-systems. The extrapolated pseudo-ternary system was further optimised based on novel experimental data obtained from DSC measurements. The assessed pseudo-ternary parameters (in J/mol) are:

$$g^{001}_{UK(Na)} = 2000. \tag{13}$$

4. Results

4.1. Phase Equilibria Determination of the Pseudo-Binary NaF-UF$_4$ and KF-UF$_4$ Mixtures

The phase equilibria temperatures experimentally obtained in this study by DSC for the NaF-UF$_4$ and KF-UF$_4$ system are presented in Tables 3 and 4 and in Figures 2 and 3, respectively. The type of equilibria were identified by the phase diagram assessment and comparison to earlier studies [15,16]. For comparison, the equilibrium temperatures calculated from the thermodynamic assessment performed in this study are shown in Tables 3 and 4 as well. They demonstrate good agreement with the experimental data for the whole composition range.

Table 3. Experimental phase equilibria and temperatures obtained by DSC for the NaF-UF$_4$ system and the calculated transition temperatures at these compositions for comparison.

x (UF$_4$)/mol%	Type of Equilibria	Temperature/K	
		Experiment	Calculation
0.100	Formation of Na$_3$[UF$_7$]	737 ± 5 K	738
	α − β transition of Na$_3$[UF$_7$]	825 ± 5 K	823
	Eutectic	887 ± 5 K	888
	Liquidus	1201 ± 15 K	1198
0.150	Formation of Na$_3$[UF$_7$]	738 ± 5 K	738
	α–β transition of Na$_3$[UF$_7$]	825 ± 5 K	823
	Eutectic	885 ± 5 K	888
	Liquidus	1120 ± 15 K	1122
0.175	Formation of Na$_3$[UF$_7$]	738 ± 5 K	738
	α–β transition of Na$_3$[UF$_7$]	826 ± 5 K	823
	Eutectic	884 ± 5 K	888
	Liquidus	1064 ± 15 K	1064
0.201	Formation of Na$_3$[UF$_7$]	739 ± 5 K	738
	unidentified	761 ± 15 K	n.a.
	α–β transition of Na$_3$[UF$_7$]	824 ± 5 K	823
	Eutectic	886 ± 5 K	888
	Liquidus	974 ± 15 K	980
0.250	Formation of Na$_3$[UF$_7$]	736 ± 5 K	738
	unidentified	770 ± 15 K	n.a.
	α–β transition of UNa$_3$F$_7$	820 ± 5 K	823
	Melting	887 ± 5 K	910

Table 3. *Cont.*

x (UF$_4$)/mol%	Type of Equilibria	Temperature/K	
		Experiment	Calculation
0.280	Formation of Na$_3$[UF$_7$]	733 ± 5 K	738
	unidentified	770 ± 15 K	n.a.
	α–β transition of Na$_3$[UF$_7$]	819 ± 5 K	823
	Eutectic	884 ± 5 K	894
0.299	Formation of Na$_3$[UF$_7$]	734 ± 5 K	738
	unidentified	775 ± 15 K	n.a.
	α–β transition of Na$_3$[UF$_7$]	819 ± 5 K	823
	Eutectic	882 ± 5 K	894
	Liquidus	921 ± 15 K	915
0.333	Peritectic	918 ± 5 K	926
0.371	Formation of Na$_5$[U$_3$F$_{17}$]	893 ± 5 K	891
	Peritectic	925 ± 5 K	926
	Liquidus	952 ± 15 K	960
0.400	Formation of Na$_5$[U$_3$F$_{17}$]	894 ± 5 K	891
	Peritectic	942 ± 5 K	943
	Liquidus	977 ± 15 K	978
0.430	Formation of Na$_5$[U$_3$F$_{17}$]	890 ± 5 K	891
	Peritectic	944 ± 5 K	943
	Liquidus	992 ± 15 K	990
0.466	Melting	988 ± 5 K	993
0.499	Eutectic	951 ± 5 K	952
	Liquidus	997 ± 15 K	990
0.559	Eutectic	951 ± 5 K	952
0.601	Eutectic	950 ± 5 K	952
	Liquidus	1007 ± 15 K	1015
0.633	Stability limit of Na[U$_2$F$_9$]	942 ± 5 K	936
	Eutectic	953 ± 5 K	952
	Liquidus	1087 ± 15 K	1081
0.667	Eutectic	947 ± 5 K	952
	Liquidus	1134 ± 15 K	1128
0.700	Stability limit of Na[U$_2$F$_9$]	937 ± 5 K	936
	Eutectic	947 ± 5 K	952
	Liquidus	1160 ± 15 K	1161
0.802	Stability limit of Na[U$_2$F$_9$]	933 ± 5 K	936
	Eutectic	946 ± 5 K	952
	Liquidus	1231 ± 15 K	1230
0.901	Eutectic	948 ± 5 K	952
	Liquidus	1273 ± 5 K	1275

Table 4. Experimental phase equilibria and temperatures obtained by DSC in the KF-UF$_4$ system and the calculated transition temperatures at these compositions for comparison.

x (UF$_4$)/mol%	Type of Equilibria	Temperature/K	
		Experiment	Calculation
0.050	Eutectic	989 ± 5 K	988
	Liquidus	1103 ± 5 K	1102
0.100	Eutectic	992 ± 5 K	988
	Liquidus	1066 ± 5 K	1045
0.150	Eutectic	993 ± 5 K	988
	Liquidus	1018 ± 5 K	1045
0.200	Eutectic	992 ± 5 K	988
	Liquidus	1170 ± 5 K	1172
0.250	Congruent melting	1218 ± 5 K	1217
0.300	Formation of K$_2$[UF$_6$]	704 ± 15 K	702
	α–β transition of K$_2$[UF$_6$]	854 ± 5 K	855
	Peritectic	1016 ± 5 K	1028
	Liquidus	1188 ± 5 K	1181
0.333 *	Formation of K$_2$[UF$_6$]	700 ± 15 K	702
	α–β transition of K$_2$[UF$_6$]	855 ± 5 K	855
	Peritectic	1026 ± 5 K	1028
0.385	Formation of K$_2$[UF$_6$]	705 ± 15 K	702
	α–β transition of K$_2$[UF$_6$]	882 ± 5 K	855
	Eutectic	1013 ± 5 K	1026
	Liquidus	1039 ± 5 K	1038
0.400	Formation of K$_2$[UF$_6$]	701 ± 15 K	702
	α–β transition of K$_2$[UF$_6$]	854 ± 5 K	855
	Eutectic	998 ± 5 K	1026
	Liquidus	1050 ± 5 K	1049
0.430	Formation of K$_2$[UF$_6$]	706 ± 15 K	702
	α–β transition of K$_2$[UF$_6$]	881 ± 5 K	855
	Eutectic	1002 ± 5 K	1026
	Liquidus	1062 ± 5 K	1062
0.462	Melting of K$_7$[U$_6$F$_{31}$]	1056 ± 5 K	1068
0.500	Eutectic	995 ± 5 K	1019
	Liquidus	1047 ± 15 K	1062
0.545	Eutectic	1016 ± 5 K	1019
	Liquidus	1049 ± 15 K	1040
0.573	Eutectic	1018 ± 5 K	1019
0.603	Eutectic	1005 ± 5 K	1019
	Liquidus	1033 ± 15 K	1028
0.667	Eutectic	1014 ± 5 K	1019
	Peritectic	1032 ± 5 K	1039
	Liquidus	1076 ± 15 K	1065

Table 4. *Cont.*

x (UF$_4$)/mol%	Type of Equilibria	Temperature/K	
		Experiment	**Calculation**
0.702	Peritectic	1031 ± 5 K	1039
	Liquidus	1122 ± 15 K	1105
0.741	Peritectic	1032 ± 5 K	1039
	Unidentified **	1075 ± 15 K	n.a.
	Liquidus	1150 ± 15 K	1150
0.800	Peritectic	1027 ± 5 K	1039
	Unidentified **	1175 ± 15 K	n.a.
	Liquidus	1193 ± 15 K	1201
0.850	Peritectic	1028 ± 5 K	1039
	Unidentified **	1073 ± 15 K	n.a.
	Liquidus	1235 ± 15 K	1237
0.900	Peritectic	1060 ± 5 K	1039
	Liquidus	1265 ± 15 K	1266

* Liquidus not detected, ** could be another peritectic due to a formation of another U-rich intermediate compound, which would need to be confirmed by another technique (e.g., high temperature XRD).
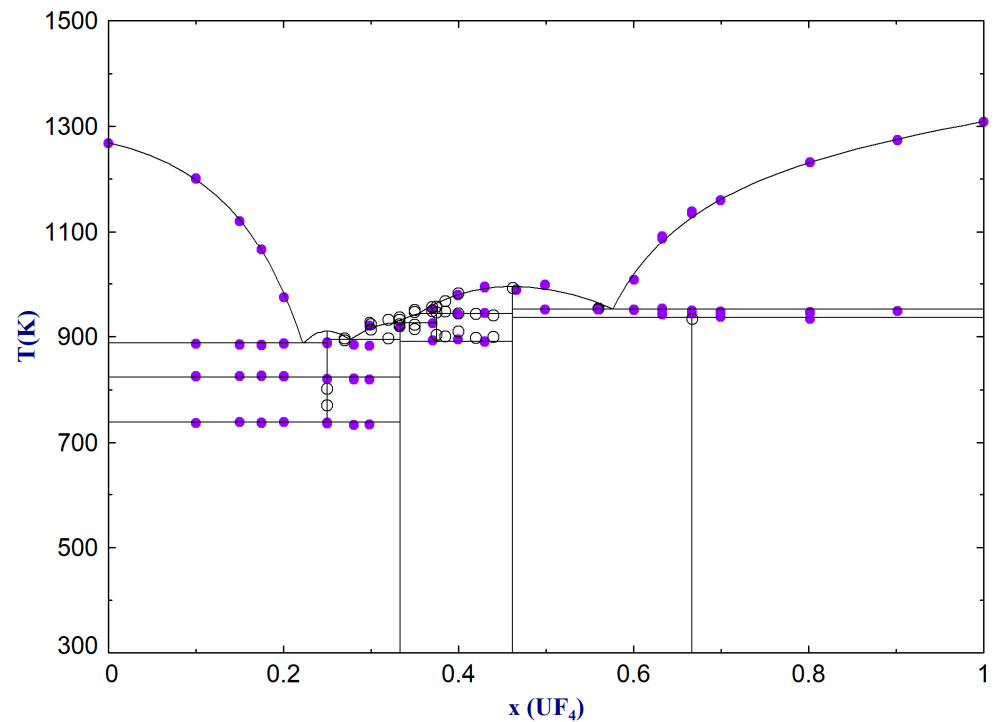
Figure 2. The calculated NaF-UF$_4$ phase diagram superimposed with our experimental data (purple solid circles) and experimental data from Barton et al. [15] (hollow circles).
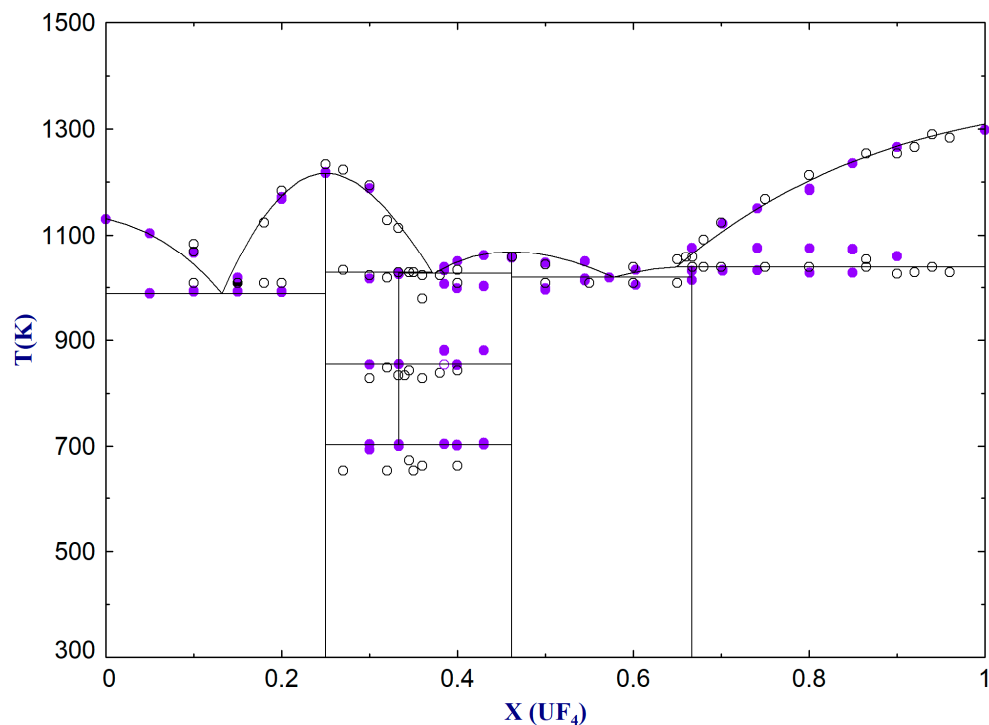
Figure 3. The calculated KF-UF$_4$ phase diagram superimposed with our experimental data (purple solid circles) and experimental data from Thoma et al. [16] (hollow circles).

4.2. Phase Equilibria Determination of the Pseudo-Ternary NaF-KF-UF$_4$ Mixtures

Twelve pseudo-ternary compositions were measured with DSC to evaluate the liquidus behaviour of the NaF-KF-UF$_4$ system. The obtained data of the liquidus points of all measured compositions are reported in Table 5 and graphically represented in Figure 4. Similar to the two studied pseudo-binary systems the calculated temperatures based on our thermodynamic assessment are provided for comparison. Although other types of equilibria (other than the here presented liquidus equilibria) were detected during DSC measurements, additional complementary analyses would be required to clearly identify the type of equilibria. The confirmation of the nature of the invariant equilibria for most of the measured transitions was identified for potential future work. As this study focuses on the melting point behaviour of the pseudo-ternary system, which is of great importance for the MSR systems, the obtained experimental data on the liquidus behaviour provides the right benchmark. Only for one selected composition (close to the suggested lowest pseudo-ternary eutectic point) all equilibria were investigated to clarify the solidus temperature. More details are given in the discussion section.

Table 5. Experimentally determined liquidus equilibria of the NaF-KF-UF$_4$ pseudo-ternary system obtained by DSC and calculated liquidus temperatures at these compositions for comparison.

X (NaF)	X (KF)	X (UF$_4$)	T$_{liquidus}$/K	
			Experiment	Calculation
0.453	0.100	0.448	971 ± 15	950
0.101	0.450	0.449	1026 ± 15	1027
0.200	0.400	0.400	1025 ± 15	982
0.497	0.279	0.224	906 ± 15	846
0.450	0.450	0.100	1051 ± 15	1048

Table 5. *Cont.*

X (NaF)	X (KF)	X (UF₄)	$T_{liquidus}$/K	
			Experiment	Calculation
0.428	0.381	0.190	969 ± 15	925
0.537	0.210	0.253	853 ± 15	849
0.523	0.187	0.290	834 ± 15	832
0.549	0.171	0.280	845 ± 15	835
0.572	0.157	0.271	834 ± 15	836
0.601	0.136	0.263	842 ± 15	834
0.633	0.121	0.246	863 ± 15	832
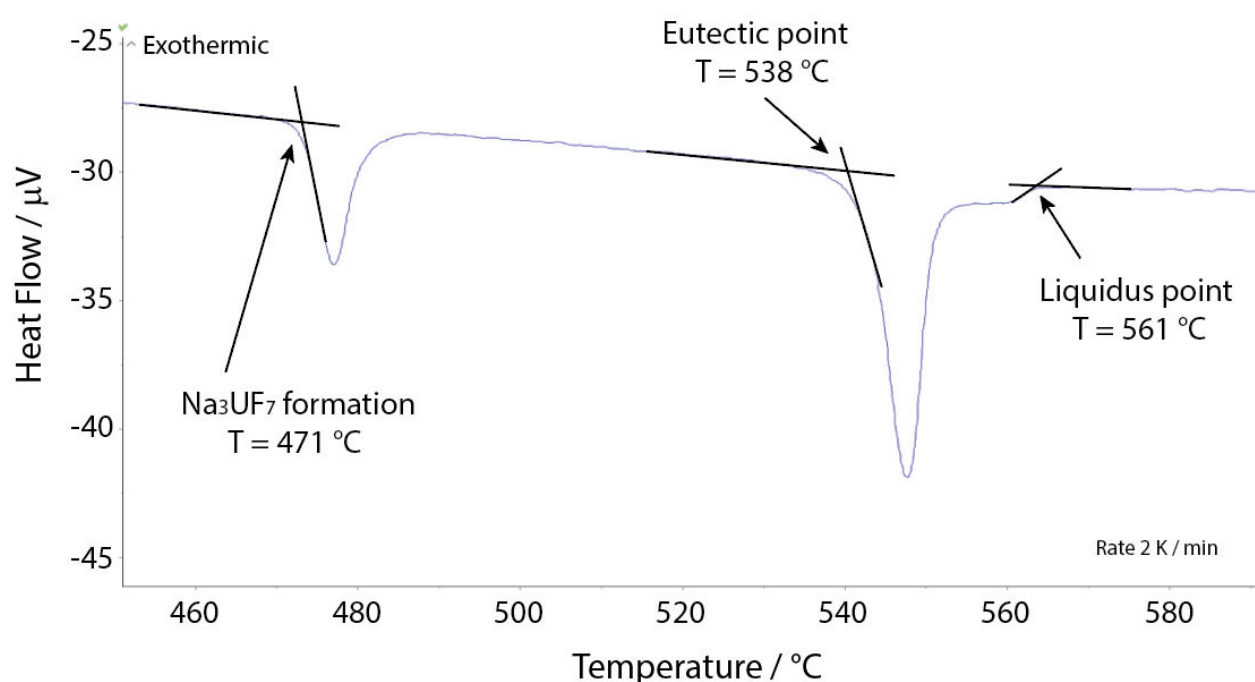
Figure 4. A DSC analysis of the phase equilibria determination of the selected NaF-KF-UF₄ (52.3-18.7-29.0 mol%) composition.

4.3. Phase Diagram Assessments of the NaF-UF₄ and KF-UF₄ Systems

Using the experimental equilibrium data obtained in this study and the data from the literature [15,16], the pseudo-binary NaF-UF₄ and KF-UF₄ phase diagrams were thermodynamically assessed. They are presented in Figures 2 and 3, respectively. Overall, our experimental data agree well with most of the data presented in the literature, only a slight discrepancy was found for the equilibrium related to the formation of the K_2UF_6 compound. We decided to use our obtained data for the modelling of the KF-UF₄ system but to verify this decision, independent measurement of different research group would be useful.

Good agreement between the measured experimental data (purple solid circles in the figures) and the model is evident, indicating a maximum discrepancy of about 15 K on the liquidus, but with most of the liquidus points within the ±5 K range.

The NaF-UF₄ system is characterised by 3 eutectic points and 2 peritectic points. The lowest eutectic is at a temperature of T = 888 K and a composition of about X(UF₄) = 22.2 mol%. The other two eutectic points are found at T = 894 K with X(UF₄) = 27.6 mol% and T = 952 K with X(UF₄) = 57.6 mol%. In total, 5 intermediate phases stabilise in the system. $Na_7[U_6F_{31}]$ and the high temperature phase $Na_3[UF_7]$ melt congruently at T = 995 K and T = 910 K, respectively. $Na_2[UF_6]$ and the second high temperature phase $Na_5[U_3F_{17}]$ exhibit peritectic

melting at T = 926 K and T = 943 K, respectively. Na[U_2F_9] decomposes into UF_4 and Na$_7$[U_6F_{31}] at 936 K.

In the KF-UF_4 system, three eutectic and two peritectic points were identified. The lowest eutectic was found at T = 988 K with X(UF_4)= 13.2 mol%, while the other eutectic points were calculated at T = 1026 K with X(UF_4)= 37.4 mol% and T = 1019 K with X(UF_4) = 57.7 mol%. Of four total intermediate compounds, K_3[UF_6] and K_7[U_6F_{31}] show congruent melting points at T = 1217 K and T = 1068 K, respectively. The high temperature stoichiometric phase K_2[UF_6] decomposes at the peritectic point at 1028 K. The second peritectic point is at 1039 K where K[U_2F_9] decomposes into UF_4 and liquid.

All calculated pseudo-binary phase equilibria of the NaF-UF_4 and KF-UF_4 systems and their exact compositions are summarised in Tables 6 and 7, respectively.

Table 6. Invariant equilibria obtained from the calculated NaF-UF_4 phase diagram.

X(UF_4)	Temperature	Equilibrium
22.2	888 K	Eutectic
25.0	738 K	Na_3UF_7 formation
25.0	823 K	α–β transition
25.0	910 K	Congruent melting
27.6	894 K	Eutectic
32.6	926 K	Peritectic
35.4	943 K	Peritectic
37.5	891 K	$Na_5U_3F_{17}$ formation
46.2	995 K	Congruent melting
57.6	952 K	Eutectic
66.7	936 K	NaU_2F_9 decomposition

Table 7. Invariant equilibria obtained from the calculated KF-UF_4 phase diagram.

X(UF_4)	Temperature	Equilibrium
13.2	988 K	Eutectic
25	1217 K	Congruent melting
33.3	702 K	K_2UF_6 formation
33.3	855 K	α–β transition
37.1	1028 K	Peritectic
37.4	1026 K	Eutectic
46.2	1068 K	Congruent melting
57.7	1019 K	Eutectic
64.9	1039 K	Peritectic

4.4. Phase Diagram Assessment of the NaF-KF-UF_4 System

The pseudo-ternary NaF-KF-UF_4 system was thermodynamically assessed based on the thermodynamic assessments of the pseudo-binary sub-systems (NaF-KF, NaF-UF_4, and KF-UF_4) and the experimental data measured in this study. The liquidus projection, together with the indicated measured data, is shown in Figure 5.
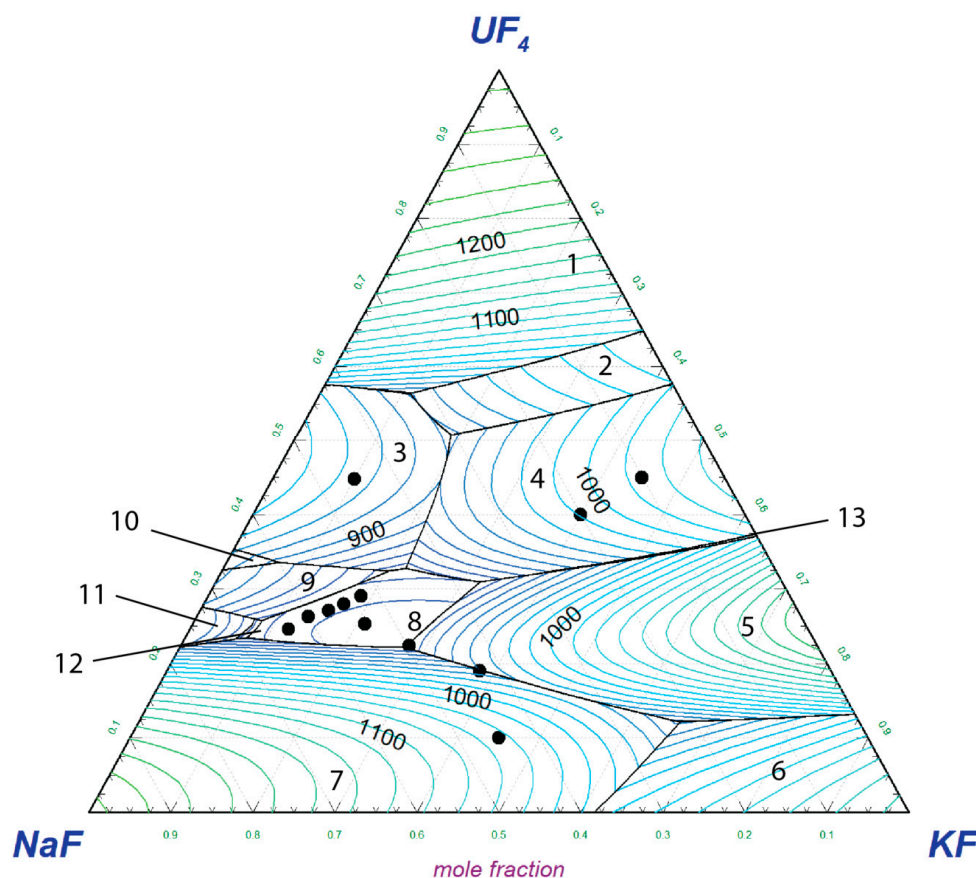
Figure 5. The calculated liquidus projection of the NaF-KF-UF$_4$ system. Isotherms are calculated in K with intervals of 20 K. The solid circles represent measured compositions and their determined liquidus temperature can be found in Table 5. The calculated primary crystallisation phase fields: (1) UF$_4$; (2) U$_2$KF$_9$; (3) Na$_7$U$_6$F$_{31}$; (4) K$_7$U$_6$F$_{31}$; (5) K$_3$UF$_7$; (6) KF_s.s.; (7) NaF_s.s.; (8) Na$_2$KUF$_7$; (9) Na$_2$UF$_6$; (10) Na$_5$U$_3$F$_{17}$; (11) α-Na$_3$UF$_7$; (12) β- Na$_3$UF$_7$; (13) K$_2$UF$_6$.

The calculated pseudo-ternary phase diagram contains 13 invariant equilibria and 13 phase fields of primary crystallisation. Two pseudo-ternary intermediate solid phases stabilise in the pseudo-ternary field; the equi-molar NaKUF$_4$ phase and the Na$_2$KUF$_7$ phase. The latter phase was revealed by a XRD analysis performed in the current study.

The calculated lowest pseudo-ternary eutectic was found at 807 K and NaF-KF-UF$_4$ (68.9-7.6-23.5 mol%) composition. The temperature is in good agreement with the experimentally determined eutectic temperature of 811 K, illustrated below in Figure 4. Although the shown example does not represent the exact composition of the eutectic point, the eutectic temperature corresponds to the onset point of the melting peak of the heat flow signal.

All calculated pseudo-ternary invariant equilibria are given in Table 8, while the primary crystallisation phases are listed in the caption of Figure 5.

Table 8. Calculated invariant equilibria, temperatures, and compositions of the NaF-KF-UF$_4$ system.

X (NaF)	X (KF)	X (UF4)	T/K	Equilibrium
32.6	11.1	56.3	898	Eutectic
30.4	18.8	50.8	893	Eutectic
21.8	66.0	12.2	893	Eutectic
60.0	6.5	33.5	891	Quasi-Peritectic

Table 8. *Cont.*

X (NaF)	X (KF)	X (UF4)	T/K	Equilibrium
31.7	36.6	31.7	855	Quasi-Peritectic
50.4	27.5	22.1	841	Quasi-Peritectic
66.8	7.2	26.0	823	Peritectic
70.6	6.2	23.2	823	Quasi-Peritectic
36.8	32.2	31.0	820	Eutectic
66.0	8.2	25.8	810	Quasi-Peritectic
47.3	20.3	32.4	810	Quasi-Peritectic
45.0	22.2	32.8	808	Eutectic
69.0	7.5	23.5	807	Eutectic

5. Discussion

The experimental re-investigation and thermodynamic modelling of the pseudo-binary $NaF-UF_4$ and $KF-UF_4$ systems provided the basis for extrapolation to the $NaF-KF-UF_4$ system. Only small ternary excess Gibbs parameters of the liquid solution were used for the thermodynamic assessment. The calculated liquidus projection was correlated with 12 experimentally measured data points (highlighted in Figure 5), which were further used for the optimisation of the pseudo-ternary system. The direct comparison of experimental and calculated liquidus temperatures is shown in Table 5. It is clear that seven points agree within a 10 K discrepancy, four points are within 45 K error, and one point has a discrepancy of 60 K. When the point with the highest discrepancy is plotted against the liquidus projection of the phase diagram, it is revealed that it belongs to a phase field with a steep liquidus increase. Hence, the composition margin for both experimental and modelling results can likely be the main cause. In this region, a small change of composition has significant impact on the melting temperature. With this note, we conclude that the preliminary assessed pseudo-ternary system provides a good estimate on the liquidus propagation.

Although fairly good general agreement between the calculated phase diagram and the measured data has been achieved, still a few items were identified for potential future investigations. First of all, as already mentioned in Section 3, we had no experimental evidence for the solid solution behaviour in the pseudo-ternary field, and therefore it was not considered in the current assessment. The presence of a solid solution might affect the liquidus surface of the pseudo-ternary field. More experimental data of the solid solution and its composition extension, with a primary focus on the phase analysis, is needed and we suggest this as a possible topic for future studies.

The same is true for the definition of stability limits of the pseudo-ternary intermediate compounds. Thoma et al. suggested that the $NaKUF_6$ intermediate compound was stable, but not many details are available on its stability range [17]. The phase diagram suggested by Thoma et al. [17] indicates a sub-liquidus stability limit (i.e., no congruent melting was observed); however the exact range is unknown. In the current study, we followed these suggestions and with novel experimental data measured in this study, we optimised the thermodynamic data of this intermediate compound leading to a stability limit of 714 K. Similarly to the solid solution, the need for more data on stability of this phase (or its presence) is suggested for future investigations.

Furthermore, we performed XRD phase analyses of one selected composition from the mid-range region (namely the $NaF-KF-UF_4$ (52.3-18.7-29.0 mol%) mixture) using a sample that has been analysed by DSC earlier and cooled down to room temperature. The obtained diffractogram is shown in Figure 6 and clearly indicates ternary equilibrium between Na_2UF_6, Na_3UF_7 and KNa_2UF_7. We took the evidence of the presence of the KNa_2UF_7 pseudo-ternary phase into consideration and optimised its thermodynamic parameters to

fit the obtained DSC data of the measured composition from that crystallisation domain. This was a key point for the NaF-KF-UF$_4$ pseudo-ternary assessment, as only with the presence of the KNa$_2$UF$_7$ pseudo-ternary compound we could reach good agreement to the measured lowest pseudo-ternary eutectic temperature.
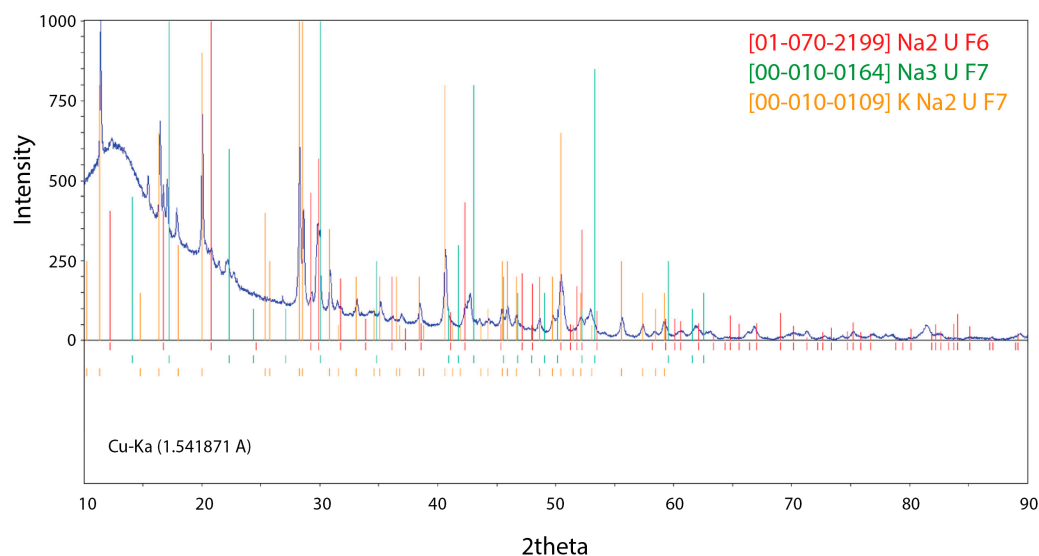

Figure 6. XRD pattern of the NaF-KF-UF$_4$ (52.3-18.7-29.0 mol%) pseudo-ternary mixture measured after the DSC experiment. Qualitative analysis was performed using Match software and PDF2 database to define the nature of phases present in the sample [20,21].

Comparing the currently assessed pseudo-ternary phase diagram with the one suggested by Thoma et al. [17], generally good agreement among the phase field domains is obtained, but a slight discrepancy between the lowest melting point (the lowest pseudo-ternary eutectic) is observed. To explain the possible source of this discrepancy, we performed careful analyses of one of the DSC runs obtained for the close-to eutectic composition, in particular the NaF-KF-UF$_4$ (52.3-18.7-29.0 mol%) composition. As shown on the heat flow signal in Figure 4, at 744.15 K (471 °C), a first transition occurs, and we consider it is due to the formation of the UNa$_3$F$_7$ compound. The thermodynamic model supports this statement, and the temperature is in close agreement with the UNa$_3$F$_7$ formation temperature measured at 738 K, as depicted in the NaF-UF$_4$ pseudo-binary phase diagram. We consider that this could be the source of the disagreement for the lowest melting temperature between the calculated pseudo-ternary phase diagram presented in this study (i.e., Figure 5) and the earlier suggested phase diagram by Thoma et al. [17] in which the lowest pseudo-ternary eutectic was estimated to be between 450 and 500 °C (i.e., 723–773 K, deduced from their figure). Since only few details were given by the authors and all data were based solely on thermal analysis, we think that the lowest melting point identified earlier could be the detected solid phase transition instead. Therefore, we suggest the eutectic temperature as the onset point of the second peak on the heat flow signal represented in Figure 4, thus 811 K (538 °C).

6. Conclusions

In this work, a substantial amount of novel experimental data on the phase equilibria of the NaF-UF$_4$, KF-UF$_4$ and NaF-KF-UF$_4$ systems was obtained. Based on these data, new pseudo-binary thermodynamic assessments of the NaF-UF$_4$ and KF-UF$_4$ systems were performed, and the optimised Gibbs energy models of the relevant phases were presented. Excellent agreement between the pseudo-binary phase equilibria data and the calculated phase diagram was achieved for both systems.

Furthermore, the full NaF-KF-UF$_4$ pseudo-ternary system was thermodynamically described. The lowest pseudo-ternary eutectic was found at 807 K (experimentally con-

firmed at 811 ± 5 K). Although we could not experimentally identify the exact lowest eutectic composition, the thermodynamic assessment points towards a composition of 68.9-7.6-23.5 mol% NaF-KF-UF$_4$. This temperature is fairly low, thus NaF and KF might serve as alternative components to LiF. Further research on this particular system is recommended to confirm the composition of the lowest eutectic point and to fully determine the stability range of pseudo-ternary solid solutions and pseudo-ternary intermediate phases.

With the few identified issues left for further research, the thermodynamic assessment of the full NaF-KF-UF$_4$ system presented in this study is a valuable contribution for further extension of the JRCMSD thermodynamic database. It describes well most of the phase field regions and provides a detailed experimental investigation of the surrounding region of the lowest melting point. The JRCMSD thermodynamic database, with this extension, can serve, e.g., nuclear regulators for their thermodynamic properties predictions needed for safety assessments. At the same time, it may be consulted by companies developing molten salt reactor technologies for the fuel composition optimisation of their multi-component fuel mixture.

Appendix A

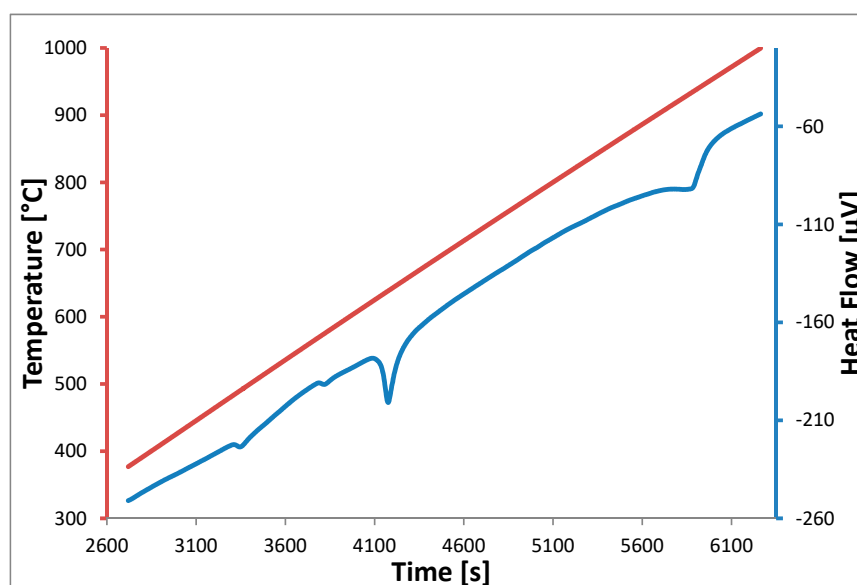**Figure A1.** Experimental DSC signal of a representative heating cycle of a NaF-UF4 sample with X(UF4) = 10mol%. The four equilibria are at 737 ± 5 K formation of Na3[UF7], at 825 ± 5 K α − β transition of Na3[UF7], at 887 ± 5 K eutectic equilibrium and at 1201 ± 15 K liquidus point.

Table 1. Intermediate NaF-UF$_4$ compositions subjected to DSC measurements within this study.

Nr.	X (UF$_4$)/mol Fraction	m (Mixture)/mg	Nr.	X (UF$_4$)/mol Fraction	m (Mixture)/mg
1	0.100	115.4 ± 0.2	11	0.430	110.3 ± 0.2
2	0.150	111.9 ± 0.2	12	0.466	112.6 ± 0.2
3	0.175	110.7 ± 0.2	13	0.499	106.8 ± 0.2
4	0.201	114.3 ± 0.2	14	0.559	110.3 ± 0.2
5	0.250	107.2 ± 0.2	15	0.601	105.8 ± 0.2
6	0.280	108.1 ± 0.2	16	0.633	111.9 ± 0.2
7	0.299	113.6 ± 0.2	17	0.667	115.2 ± 0.2
8	0.333	110.2 ± 0.2	18	0.700	103.4 ± 0.2
9	0.371	101.7 ± 0.2	19	0.802	109.1 ± 0.2
10	0.400	103.6 ± 0.2	20	0.901	101.7 ± 0.2

Table 2. Intermediate KF-UF$_4$ compositions subjected to DSC measurements within in this study.

Nr.	X (UF$_4$)/mol Fraction	m (Mixture)/mg	Nr.	X (UF$_4$)/mol Fraction	m (Mixture)/mg
1	0.050	114.4 ± 0.2	12	0.500	104.6 ± 0.2
2	0.100	108.9 ± 0.2	13	0.545	99.7 ± 0.2
3	0.150	115.1 ± 0.2	14	0.573	107.4 ± 0.2
4	0.200	107.5 ± 0.2	15	0.603	108.0 ± 0.2
5	0.250	106.5 ± 0.2	16	0.667	108.3 ± 0.2
6	0.300	103.6 ± 0.2	17	0.702	97.9 ± 0.2
7	0.333	109.7 ± 0.2	18	0.741	108.9 ± 0.2
8	0.385	111.4 ± 0.2	19	0.800	101.6 ± 0.2
9	0.400	106.2 ± 0.2	20	0.850	104.1 ± 0.2
10	0.430	107.1 ± 0.2	21	0.900	112.7 ± 0.2
11	0.462	103.9 ± 0.2			

References

1. Serp, J.; Allibert, M.; Beneš, O.; Delpech, S.; Feynberg, O.; Ghetta, V.; Heuer, D.; Holcomb, D.; Ignatiev, V.; Kloosterman, J.L.; et al. The molten salt reactor (MSR) in generation IV: Overview and perspectives. *Prog. Nucl. Energy* **2014**, *77*, 308–319. [CrossRef]
2. Beneš, O.; E-Merle-Lucotte; Capelli, E.; Allibert, M.; Brovchenko, M.; Heuer, D.; Konings, R.J.M.; Delpech, S. *Deliverable D3.7 Selection of the MSFR Fuel Salt Composition: Evaluation and Viability of Liquid Fuel Fast Reactor System (EVOL)*; Joint Research Center of the European Commission Karlsruhe: Karlsruhe, Germany, 2013.
3. Robertson, R.C. *MSRE Desing and operation Report Part 1: Description of reactor Desing*; ORNL-TM 728; Oak Ridge National Laboratory: Oak Ridge, TN, USA, 1965.
4. Allibert, M.; Aufiero, M.; Brovchenko, M.; Delpech, S.; Ghetta, V.; Heuer, D.; Laureau, A.; Merle-Lucotte, E. Molten salt fast reactors. In *Handbook of Generation IV Nuclear Reactor*; Woodhead Publishing: Sawston, UK, 2016; pp. 157–188. [CrossRef]
5. Ignatiev, V.V.; Feynberg, O.S.; Zagnitko, A.V.; Merzlyakov, A.V.; Surenkov, A.I.; Panov, A.V.; Subbotin, V.G.; Afonichkin, V.K.; Khokhlov, V.A.; Kormilitsyn, M.V. Molten-salt reactors: New possibilities, problems and solutions articles. *At. Energy* **2012**, *112*, 157–165. [CrossRef]
6. JRCMSD. *Thermodynamic Database on Molten Salt Reactor Systems*; European Commission, Joint Research Centre: Karlsruhe, Germany, 2021.
7. Grimes, W.R.; Cuneo, D.R.; Blankenship, F.F.; Keilholtz, G.W.; Poppendick, H.F.; Robinson, M.T. Chemical aspects of molten-fluoride-salt reactor fuels. In *Fluid Fuel Reactors*; Addison-Wesley Publishing Company, Inc.: Reading, MA, USA, 1958; pp. 569–594.
8. Williams, D.F. *Assessment of Candidate Molten Salt Coolants for the NGNP/NHI Heat-Transfer Loop*; ORNL/TM-2006/69; Oak Ridge National Laboratory: Oak Ridge, TN, USA, 2006.
9. Cohen, S.I.; Powers, W.D.; Greene, N.D. *A Physical Property Summary for ANP Fluoride Mixtures*; ORNL-2150; Oak Ridge National Laboratory: Oak Ridge, TN, USA, 1952.

10. Beneš, O.; Konings, R.J.M. Molten salt reactor fuel and coolant. In *Comprehensive Nuclear Materials*; Elsevier Science: Amsterdam, The Netherlands, 2012; pp. 359–389. [CrossRef]

11. Kurnakow, N.S.; Żmcżużnyj, S.F. Isomorphismus der Kalium- und Natriumverbindungen, Zeitschrift Für Anorg. *Chemie* **1907**, *52*, 186–201. [CrossRef]

12. Dombrovskaya, N.S.; Koloskova, Z.A. Double decomposition in the absence of a solvent. XXXVI. Irreversible reciprocal system of sodium and potassium fluorides and bromides. *Izv. Sekt. Fiz. Anal.* **1938**, *10*, 28.

13. Holm, J.L. Phase relations in the systems NaF-LiF, NaF-KF, and NaF-RbF. *Acta Chem. Scand.* **1965**, *19*, 638–644. [CrossRef]

14. Beneš, O.; Konings, R.J.M. Thermodynamic evaluation of the MF-LaF$_3$ (M=Li, Na, K, Rb, Cs) systems. *Calphad* **2008**, *32*, 121–128. [CrossRef]

15. Barton, C.J.; Friedman, H.A.; Grimes, W.R.; Insley, H.; Moore, R.E.; Thoma, R.E. Phase equilibria in the alkali fluoride-uranium tetrafluoride fused salt systems: I, The systems LiF-UF$_4$ and NaF-UF$_4$. *J. Am. Ceram. Soc.* **1958**, *41*, 63–69. [CrossRef]

16. Thoma, R.E.; Insley, H.; Landau, B.S.; Friedman, H.A.; Grimes, W.R. Phase equilibria in the alkali fluoride-uranium tetrafluoride fused salt systems: II, The systems KF-UF$_4$ and RbF-UF$_4$. *J. Am. Ceram. Soc.* **1958**, *41*, 538–544. [CrossRef]

17. Thoma, R.E.; Barton, C.J.; Blakerly, J.P.; Moore, R.E.; Nessle, G.J.; Insley, H.; Friedman, H.A. The system NaF-KF-UF4. In *Phase Diagrams Nuclear Reactor Materials*; ORNL-2548; Oak Ridge National Laboratory: Oak Ridge, TN, USA, 1959; p. 103.

18. Souček, P.; Beneš, O.; Claux, B.; Capelli, E.; Ougier, M.; Tyrpekl, V.; Vigier, J.-F.; Konings, R.J.M. Synthesis of UF$_4$ and ThF$_4$ by HF gas fluorination and re-determination of the UF$_4$ melting point. *J. Fluor. Chem.* **2017**, *200*, 33–40. [CrossRef]

19. Chase, M.W., Jr. *NIST-JANAF Thermochemical Tables*, 4th ed.; American Institute of Physics: College Park, MD, USA, 1998.

20. International Centre for Diffraction Data. PDF-2 Database. 2018. Available online: www.icdd.com (accessed on 16 August 2021).

21. Putz, H.; Brandenburg, K. Match Software Version 1.11f, Crystal Impact GbR. 2011. Available online: https://www.crystalimpact.de/match (accessed on 16 August 2021).

22. Black, D.R.; Windover, D.; Henins, A.; Filliben, J.; Cline, J.P. Certification of standard reference material 660B. *Powder Diffr.* **2011**, *26*, 155–158. [CrossRef]

23. Beneš, O.; Konings, R.J.M.; Wurzer, S.; Sierig, M.; Dockendorf, A. A DSC study of the NaNO$_3$-KNO$_3$ system using an innovative encapsulation technique. *Thermochim. Acta* **2010**, *509*, 62–66. [CrossRef]

24. Tosolin, A.; Souček, P.; Beneš, O.; Vigier, J.-F.; Luzzi, L.; Konings, R.J.M. Synthesis of plutonium trifluoride by hydro-fluorination and novel thermodynamic data for the PuF$_3$-LiF system. *J. Nucl. Mater.* **2018**, *503*, 171–177. [CrossRef]

25. Bale, C.W.; Bélisle, E.; Chartrand, P.; Decterov, S.A.; Eriksson, G.; Gheribi, A.E.; Hack, K.; Jung, I.H.; Kang, Y.B.; Melançon, J.; et al. FactSage thermochemical software and databases, 2010–2016. *Calphad* **2016**, *54*, 35–53. [CrossRef]

26. Konings, R.J.M.; van der Meer, J.P.M.; Walle, E. *Chemical Aspects of Molten Salt Reactor Fuel*; Techical Report; Institute for Transuranium Elements (ITU): Karlsruhe, Germany, 2005.

27. Konings, R.J.M.; Morss, L.R.; Fuger, J. Thermodynamic properties of actinides and actinide compounds. In *The Chemistry of the Actinide and Transactinide Elements*; Morss, L.R., Edelstein, N.M., Fuger, J., Eds.; Springer: Dordrecht, The Netherlands, 2006; pp. 2113–2224. [CrossRef]

28. Pelton, A.D.; Chartrand, P.; Eriksson, G. The modified quasi-chemical model: Part IV. *Two-sublattice quadruplet approximation*. *Metall. Mater. Trans. A Phys. Metall. Mater. Sci.* **2001**, *32*, 1409–1416. [CrossRef]

29. Chartrand, P.; Pelton, A.D. The modified quasi-chemical model: Part III. Two sublattices. *Metall. Mater. Trans. A Phys. Metall. Mater. Sci.* **2001**, *32*, 1397–1407. [CrossRef]